Nanosilica Filled Poly(glycerol-sebacate-citrate) Elastomers with Improved Mechanical Properties, Adjustable Degradability, and Better Biocompatibility

Yan Wu,[1] Rui Shi,[2] Dafu Chen,[2] Liqun Zhang,[1] Wei Tian[2]

[1]*Key Laboratory of Beijing City for Preparation and Processing of Novel Polymer Materials, Beijing University of Chemical Technology, Beijing 10029, China*
[2]*Laboratory of Bone Tissue Engineering of Beijing Research Institute of Traumatology and Orthopaedics, Beijing 100035, China*

Received 27 August 2010; accepted 22 March 2011
DOI 10.1002/app.34556
Published online 19 August 2011 in Wiley Online Library (wileyonlinelibrary.com).

ABSTRACT: Modified nano-fumed silica (mn-silica)/poly(glycerol-sebacate-citrate), in which mn-silica loadings varied from 0 to 20 phr, were prepared by *in situ* polymerization and surface modification. The influence of mn-silica loadings on the structure and properties of the composites was studied. Scanning electron microscope (SEM) and transmission electron microscope (TEM) photos showed that the mn-silica dispersed well as nano-scale network in the matrix, and exhibited good interfacial bonding with the matrix. The mn-silica filled composites exhibited excellent comprehensive properties relative to the unfilled elastomers. Specially, the tensile strength improved from 0.9 MPa to 5.3 MPa. Results of the *in vitro* degradation test suggested that mn-silica loading could adjust the degradation rate of the composites in simulated body fluid solution. The MTT colorimetry with L929 cells substantiated that the introduction of mn-silica weakened the cytotoxicity of elastomers and made the composites accepted as qualified biomedical materials. © 2011 Wiley Periodicals, Inc. J Appl Polym Sci 123: 1612–1620, 2012

Key words: biodegradable; polyester elastomer; *in situ* polymerization; nanocomposites; biocompatibility

INTRODUCTION

As many tissues in the body have elastomeric properties, bioelastomers were widely used in medical field for good flexibility and biocompatibility. Several biodegradable polyester elastomers have been reported, poly(glycerol sebacate),[1–9] poly(polyol sebacate),[10,11] poly(diol citrate),[12,13] poly(ester amide),[14] polycaprolactone,[15] poly(ester-carbonate),[16] for instance. Our group has synthesized series of polyester elastomers using two or three kinds of the following monomers: sebacic acid, glycerol, 1,2-propanediol, 1,3-propanediol, and citric acid.[6–9,17–19] These bioelastomers exhibited many advantages, such as nontoxic, readily available and inexpensive monomers, high flexibility of molecular design, good processability, and controllable mechanical and biodegradable properties. Nevertheless, the problem of their low mechanical strengths motivates the research on the reinforcement of such bioelastomers. Nano-reinforcement by employing nanoparticles is necessary for high-efficiency reinforcement of elastomeric polymer materials, which was already proven by numerous researches and industrial applications.[20–23] Liu et al. and Lei et al.[24,25] reported the preparation of multi-walled carbon nanotube or nano-hydroxyapatite filled elastomeric nanocomposites with improved mechanical properties. However, there has been a dearth of research on the design and preparation of bioelastomers filled with nanosilica, although nanosilica is a kind of common and inexpensive filler[26–28] which has been approved for food, cosmetic as well as medical uses by the US FDA.[29] Herein, we describe the preparation and characterization of a novel bioelastomer nanocomposite, modified nanosilica/poly(glycerol-sebacate-citrate) (mn-SiO_2/PGSC), which has potential use in tissue engineering and drug delivery. Two strategies were adopted to improve the dispersion of nanosilica: (1) surface modification of nanosilica with KH-792 coupling agent, which has good compatibility with both the monomers and elastomers, and (2) *in situ* polymerization, which has been proved to be more effective than the traditional mechanical mixing, owing to the wetting and penetrating of monomers

Correspondence to: L. Zhang (zhanglq@mail.buct.edu.cn) or W. Tian (tianweia@163bj.com).

Contract grant sponsor: Beijing Natural Science Foundation as key project; contract grant number: 2061002.
Contract grant sponsor: National Distinguished Young Scientist Fund of Nature Science Foundation Committee, China; contract grant number: 50725310.
Contract grant sponsor: key project of Nature Science Foundation Committee, China; contract grant number: 50933001.

together with long-time mechanical shear. As a result, mn-silica dispersed well as nano-scale network in the matrix and mechanical properties of the composites improved significantly with the increase of nanosilica loadings. The influence of mn-silica loadings on the structure and other properties of the nanocomposites were also researched. It is worth pointing out that the introduction of mn-silica weakened the cytotoxicity of elastomers, and made the composites accepted as qualified biomedical materials.

EXPERIMENTAL

Materials

Nano-fumed silica, with diameters around 25–35 nm, was obtained from Jilin Shuangji Chemical Limited Corp. *N*-Aminoethyl-γ-aminopropyltrimethoxy silane (KH-792) (purity > 99.0%) was bought from Beijing Shenda Silane Coupling Agent Limited Corp. Sebacic acid (SA) (purity > 99.5%) was obtained from the Guangfu Fine Chemical Institute of Tianjin. Glycerol (purity > 99.0%) and citric acid (CA) monohydrate (purity > 99.0%) were purchased from Beijing Chemical Plant. Tetrahydrofuran (purity > 99.8%) was bought from Beijing Century Red-Star Chemical Limited Corp. Simulated body fluid (SBF) solution was made up in the lab.[30] Mouse fibroblast cell line (L-929 cells) was provided by the cell bank of Peking University Health Science Center. The culture medium named Dulbecco's modified Eagle Medium (DMEM) with 10% calf serum was purchased from Invitrogen Corp. GIBCO.

Modification of nano-fumed silica

KH-792 and nano-fumed silica were mixed at a weight ratio of 8/100 in a high speed disintegrating machine for 5 min, then heated at 150°C for half an hour to obtain the modified nano-fumed silica (mn-silica).

Preparation of mn-SiO_2/PGSC

Glycerol and SA were premixed at a molar ratio of 1/1 in a three-neck round-bottom flask. They were heated to melt at 120°C under a pressure of 2 kPa for 1 h. Then the various loadings (0–20 phr) of mn-silica were added to the flask under atmosphere pressure, and the pressure was adjusted to 1 kPa. After 20 h, PGS prepolymers mixed with mn-silica were formed. Subsequently, CA was added to the system according to a molar ratio of 2/2/0.3 (Glycerol/SA/CA). The mixtures continued reacting for 1 h under the condition of 120°C and 1 kPa. Additionally, the mixtures were mechanically stirred and purged with nitrogen during the whole reaction progress. Finally, the above mixtures with various loadings of mn-silica were transferred to polyfluortetraethylene molds and thermally cured at 120°C under the atmospheric pressure, obtaining series of mn-SiO_2/PGSC bioelastomer. The loadings of mn-silica were relative contents as the weight of PGSC was defined as 100 phr. Additionally, representative composites mentioned below referred to the composites whose loadings of mn-silica were 0, 6, 12, and 20 phr. The resulting films were transparent, as shown in Figure 1.

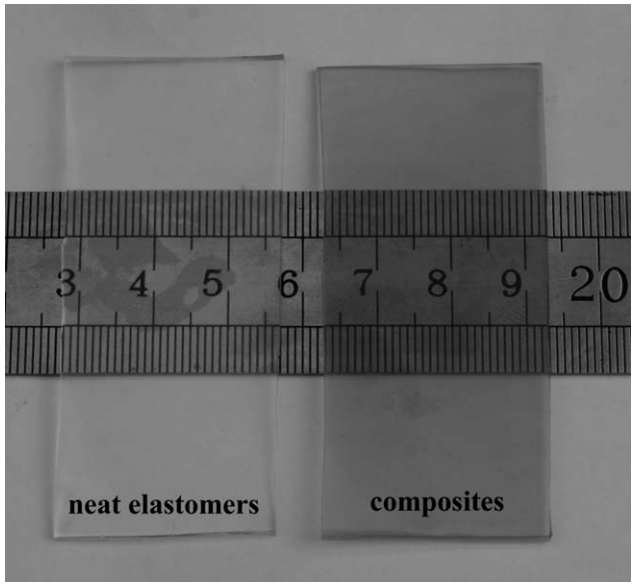

Figure 1 Surface morphologies: (1) neat elastomers; (2) composites with 20 phr mn-silica.

Characterization of the mn-SiO_2/PGSC composites

FTIR spectra of nanosilica, mn-silica, neat elastomers, and the composites with 20 phr mn-silica were recorded on the Bruker Tensor-27 spectrometer. The spectra were obtained at a resolution of 4 cm^{-1} in the range of 4000–400 cm^{-1}. Nanosilica and mn-silica were extracted in ethanol solvent for several hours to eliminate the unreacted KH-792 coupling agents and then mixed with KBr.

Morphologies of freeze-fracture surfaces of the composites with 12 phr and 20 phr mn-silica were observed by Hitachi *S*-4700 scanning electron microscope (SEM) under an acceleration voltage of 20 kV. SEM specimens were prepared by fracturing the composites in liquid nitrogen and were coated with gold before examination. Transmission electron microscope (TEM) specimens (50–70 nm thickness) were cut using a Leica EM FC6 ultramicrotome and mounted on 200 mesh copper grids before observed by Hitachi H-800 TEM.

Sol–gel compositions of the representative composites were described by sol content tests. A disc specimen (1 mm in thickness and 10 mm in diameter)

with weight of M_1 was immersed into 20 mL tetrahydrofuran solvent at 37°C for 24 h, and then dried sufficiently to constant weight of M_2. The part that dissolved in solvent was defined as sol. Thus the sol content could be calculated as follows: sol content = $(M_1 - M_2)/M_1 \times 100\%$.

Tensile tests were performed by SANS-CMT4104 testing machine (Shenzhen SANS Testing Machine Co. Ltd., China) equipped with a 50 N load cell at 21°C. The dumbbell specimens (1 mm in thickness and 2 mm in width) were pulled to break at a speed of 50 mm/min. Tensile strength, elongation at break, and Young's modulus were obtained from stress–strain curve and their values were averaged from 5 parallel specimens.

XRD patterns of the representative composites were recorded with a Rigaku model D/Max2500VB2+/PC XRD (Rigaku Co., Japan) with nickel filtered Cu-Kαradiation. The specimens were 1 mm in thickness with smooth surfaces. The scattering angles (2θ) ranges were from 10° to 60° at 5°/min.

Glass transition temperature (T_g) of the representative composites was measured with DSC Q200 (TA Instruments, New Castle, Delaware, USA). Specimens (5–10 mg) were heated at the rate of 40 °C/min from room temperature to 150°C, held for 5 min at 150°C, and then cooled to −100°C at the rate of 10 °C/min for complete quenching. Finally, the specimens were heated again from −100 to 150°C at the rate of 20 °C/min to obtain T_g, which was determined from the midpoint of the heat capacity change.

Disc specimens (1 mm in thickness and 10 mm in diameter) were immersed in weighting bottles with 20 mL SBF solution at 37°C to study the *in vitro* degradability of the representative composites. After certain degradation time, a specimen with weight of G_1 was taken out and dried sufficiently to constant weight of G_2. Thus weight loss value was calculated according to the formulation of $(G_1 - G_2)/G_1 \times 100\%$ and then averaged from two parallel specimens.

Cytotoxicity of the representative composites was evaluated using L-929 cells by MTT colorimetry shown below. The specimens were incubated in the phosphate-buffered saline solution for 8 h to decrease the effects of impurity on cells. The 1 mm thick specimens were sterilized by washing with 95% (v/v) ethanol three times and exposing to Co^{60} for 15 min. After sterilization, specimens were incubated in DMEM at a proportion of 3 cm^2/mL for 24 h at 37°C. The extract solution was then filtered (0.22 μm pore size) to eliminate the possible presence of solid particles of the material. L929 cells were cultured in DMEM with 10% (v/v) fetal bovine serum at a density of 4.0×10^4 cells/mL and plated into 96-well micrometer plates. The plates were incubated for 24 h at 37°C in a humidified atmosphere of 5% CO_2 in air. After that, the medium was replaced by the previously prepared extracted dilutions (50%, v/v) and was used as a culture medium, by itself as a control. After 2, 4, and 7 days' incubation, the cell culture was treated with MTT. 50 mL/well of MTT (5mg/mL in medium 199 without phenol red) treated specimens were incubated for further 4 h at 37°C in a humid atmosphere of 5% CO_2 in air. At this stage MTT was removed and 100 mL/well of dimethyl sulfoxide was added to dissolve the formazan crystals. The optical density (OD) was read on a multi-well microplate reader (EL 312e Biokinetics Reader) at 490 nm. Cell relative growth rate (RGR) based on the OD was calculated according to the following equation: (OD values of the experiment group)/(OD values of the negative control) × 100%. All materials were tested for a minimum of three separate experiments with comparable results.

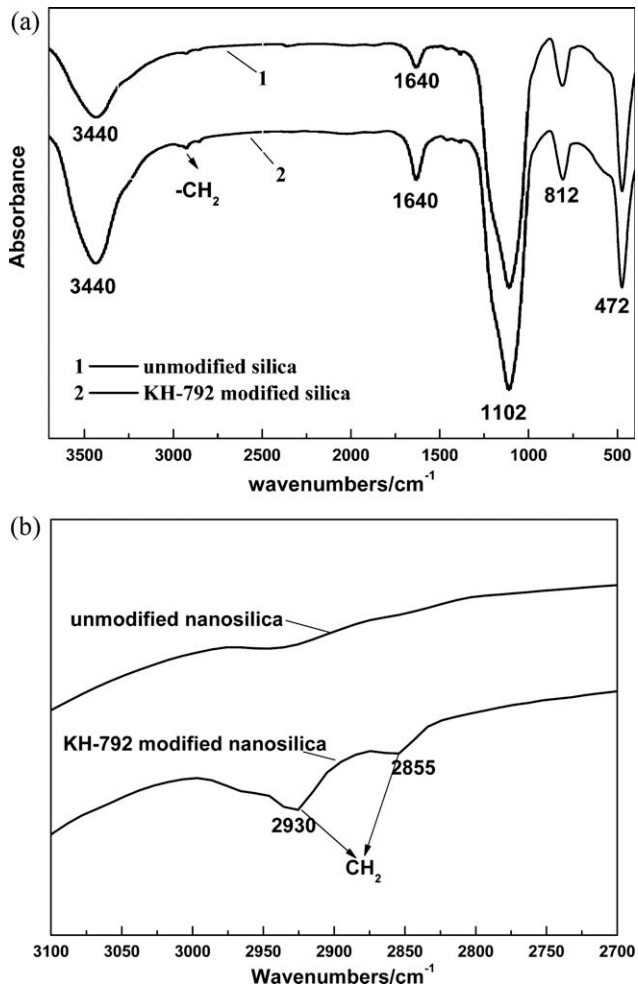

Figure 2 IR spectra of nanosilica and mn-silica. (a) Integrity spectra; (b) locally magnified spectra.

RESULTS AND DISCUSSION

FTIR spectra

The modification effect of KH-792 coupling agent on nanosilica was characterized by FTIR [Fig. 2(a)]. The

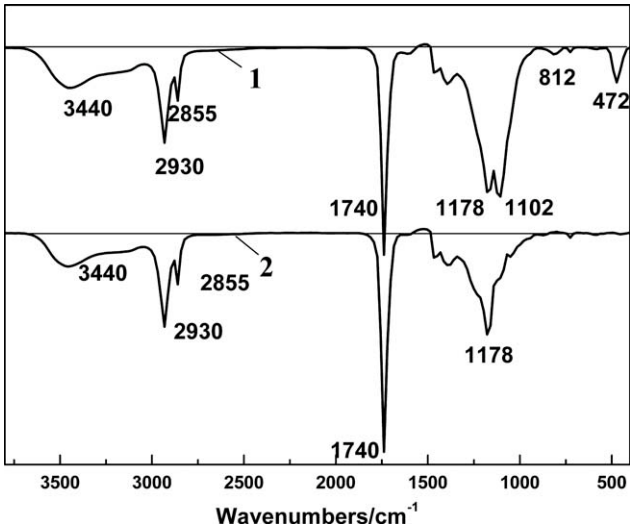

Figure 3 IR spectra: (1) with 20 phr mn-silica; (2) neat matrix.

broad peak at 3440 cm^{-1} stood for stretching vibrations of the abundant —OH groups of nanosilica. The peak at 1640 cm^{-1} was attributed to the bending vibrations of absorption water, which was inevitable during storage and use. The peaks near 1102, 812, and 472 cm^{-1} were corresponded to the vibrations of Si—O. Seen from the magnified spectra [Fig. 2(b)], —CH_2 appeared in the mn-silica corresponding to the absorption peaks at 2930 and 2855 cm^{-1}. Before the test, specimens were extracted in ethanol solvent to erase the effect of free coupling agent, hence the existence of —CH_2 belonged to KH-792 in the mn-silica validated that KH-792 was chemically bonded to silica by modification.

As shown from the spectra of composites and neat matrix (Fig. 3), the stretching vibration absorption at 1740 and 1178 cm^{-1} (corresponding to —C=O and C—O—C separately) illustrated that ester bonds formed; the broad peak near 3440 cm^{-1} (corresponding to —OH) indicated that there were many unreacted hydroxyl groups left in the system; the peaks at 2930 and 2855 cm^{-1} stood for methylene. On comparing the spectra of the composites and neat matrix, we noticed that composites presented the similar absorption peaks and close absorption

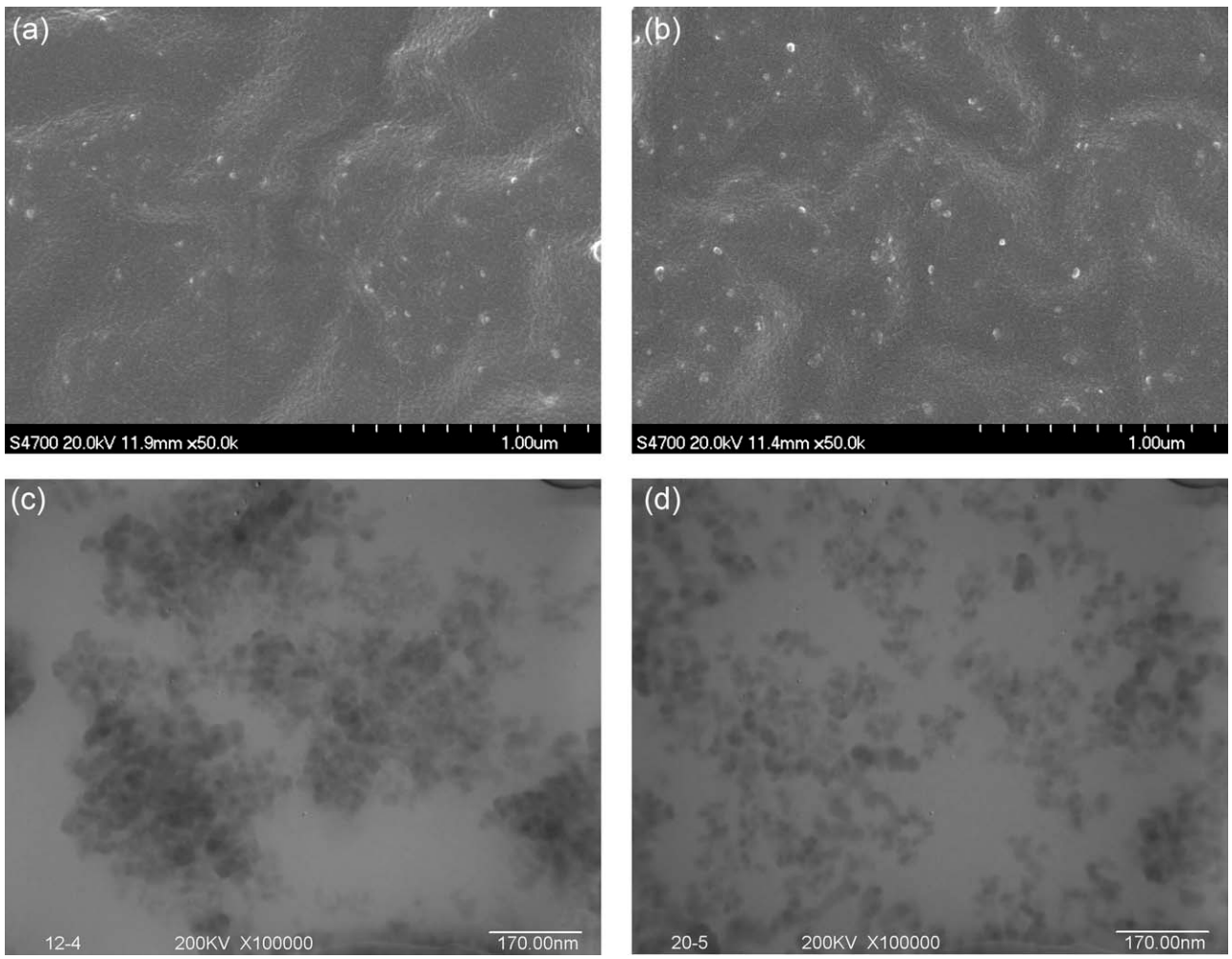

Figure 4 SEM and TEM images of the composites with 12 and 20 phr mn-silica. (a) 12 phr (SEM); (b) 20 phr (SEM); (c) 12 phr (TEM); (d) 20 phr (TEM).

TABLE I
Sol Content of Representative Composites

mn-silica loading (phr)	0	6	12	20
Sol content (%)	11.3	17.4	20.2	22.2

intensities with the matrix, except that the absorption peaks of Si—O (corresponding to 1102, 812, and 472 cm^{-1}) appeared in the composites, which indicated that mn-silica did not change the chemical structure of the matrix significantly.

Morphology of mn-SiO_2/PGSC

To assess the dispersion of mn-silica in the matrix, morphologies of the composites were observed by SEM and TEM, and the images were shown in Figure 4(a–d). SEM observation illustrated that mn-silica was well enclosed by polymers. The indistinct interfacial surface between mn-silica and polymers demonstrated good filler–polymer compatibility, owing to the strong interaction between —NH_2 of KH-792 and —OH, —COOH, —COOR of polymers. SEM and TEM images revealed that mn-silica dispersed well as nano-scale network in the matrix. That is, mn-silica was not absolutely uniformly dispersed when viewed from high magnification, while uniformly dispersed when viewed from low magnification. Preparation process of the composites might account for this phenomenon. At the last step of preparation, the mixtures were gradually cured in oven for hours without mechanical stirring, and nanoparticles in the low viscosity prepolymer might re-aggregate in small field during this process. A similar observation was reported elsewhere.[25] Additionally, more homogenous dispersion of the mn-silica was observed when increasing the loading of mn-silica. Ameer and coworkers explained similar phenomenon by the decrease in the interparticle and aggregate distance.[31] Besides, we supposed that improved viscosity of the system induced by increased mn-silica loadings, which led to stronger shear force and weaker aggregation tendency, might also contribute to more homogeneous dispersion.

Sol contents of mn-SiO_2/PGSC

Sol content can indirectly reflect the polymerization degree and chemical crosslinking density of materials. Generally, higher sol content means lower polymerization degree and chemical crosslinking density. Table I lists sol contents in the representative composites, normalized by mn-silica loadings. A trend existed that sol contents increased with the loading of mn-silica, which suggested that the loading of mn-silica decreased the chemical crosslinking densities of the polymers. The volume effect and polar force of mn-silica might be responsible for the increased resistance of polymerization.

Mechanical properties of mn-SiO_2/PGSC

Table II lists mechanical properties of the composites with various mn-silica loadings. The permanent sets of all composites were 0%, which meant that the elastomer composites presented good elastic recovery. Mechanical properties of the composites were prominently enhanced while increasing the loading of mn-silica. Especially, when 20 phr mn-silica was introduced, the tensile strength reached 5.3 MPa, which was 489% higher than unfilled elastomers. Elongations at break of the composites increased significantly as well compared to the matrix due to the nano-strengthening effect.

Liu et al.[18,19] in our laboratory reported that the tensile strengths of PGSC elastomers increased with their chemical crosslinking densities. In this experiment, sol content test aforementioned proved that the chemical crosslinking densities of polymers decreased while increasing the loading of mn-silica. However, tensile strengths of the composites improved instead. This phenomenon was related to the mechanism of elastomer reinforcement by nanoparticles. Stretched polymer chains were formed during stretching between the neighbor particles, induced by the slippage of polymer chains on the particle surface, leading to improved strength and toughness.[23]

XRD analysis

XRD curves of the composites with various mn-silica loadings were displayed in Figure 5. Short-range ordered structure was observed obviously in amorphous PGSC elastomers. The ordered arrangement degrees decreased while increasing the loading of mn-silica, which was indicated by the decrease in the intensities of diffraction peaks. Herein, the influence of mn-silica was reflected on two aspects: on one hand, the introduction of mn-silica decreased

TABLE II
Mechanical Properties of the Matrix and Nanocomposites

mn-Silica loading (phr)	0	3	6	9	12	15	20
Tensile strength (MPa)	0.9	1.6	2.4	3.1	3.6	4.0	5.3
Elongation at break (%)	33	119	109	114	117	136	93
Permanent set (%)	0	0	0	0	0	0	0

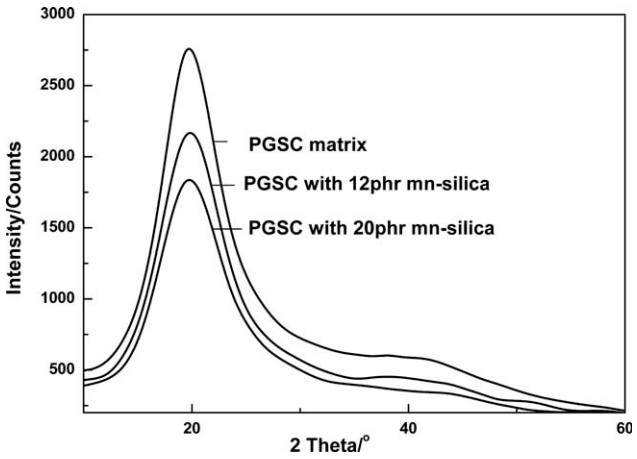

Figure 5 XRD curves of representative composites.

the chemical crosslinking density of polymers, substantiated by the sol content test; on the other hand, its polar force of —OH and —NH_2 hindered the formation of ordered structure induced by the intermolecular force between polymer chains.

Glass transition temperatures of mn-SiO_2/PGSC

The DSC heating thermograms of the representative composites are depicted in Figure 6. No crystalline melting peaks were found, which indicated that the composites were amorphous. We noticed that the T_g of the composites shifted to lower temperatures while increasing the loading of mn-silica. Generally, nanofillers may increase the T_g of materials through filler–polymer interaction, especially when the interaction is strong enough to block the segmental motion. The opposite results were because the introduction of mn-silica decreased the chemical crosslinking density and ordered arrangement degree of polymers, as mentioned above, promoting the activity of polymer chains.

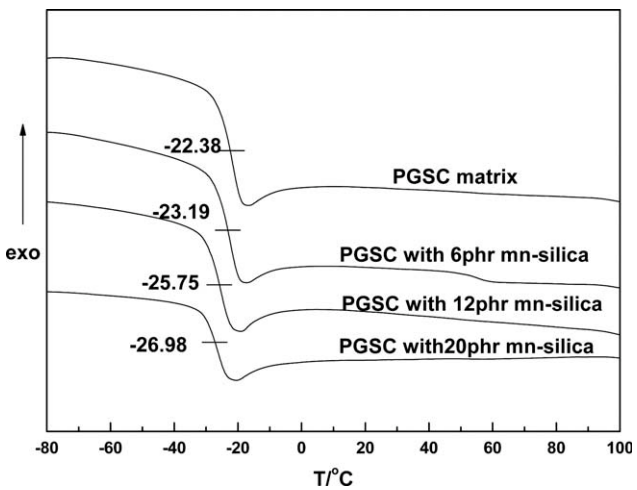

Figure 6 DSC curves of representative composites.

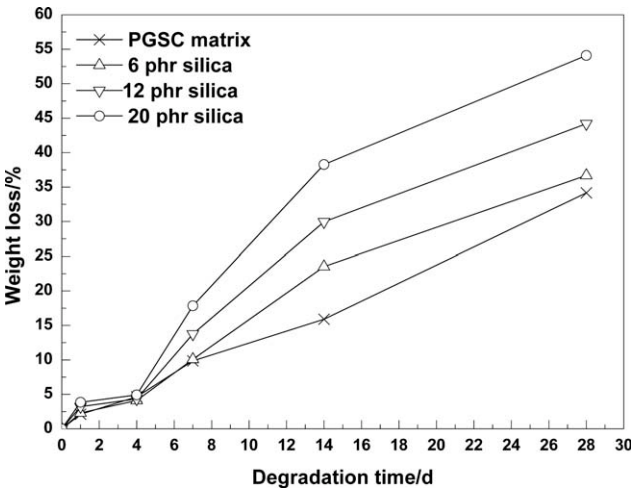

Figure 7 *In vitro* degradation weight loss–time curves of representative composites.

In vitro degradation of mn-SiO_2/PGSC

In vitro degradation of the representative composites was tested in SBF solution at 37°C. Weight losses at different degradation periods are recorded in Figure 7. It can be seen that all the composites obey similar degradation rules with neat elastomers. Generally, the degradation process could be divided into three main stages: quick weight loss in the first day, followed by equilibrium stage in the subsequent two days, and further degradation at last. The supposed degradation mechanism can be explained as follows: the sols

TABLE III
Corresponding Relationships Between the RGR Value and Cytotoxicity Grade

Grades	0	1	2	3	4	5
RGR (%)	>100	75–99	50–74	25–49	1–25	0

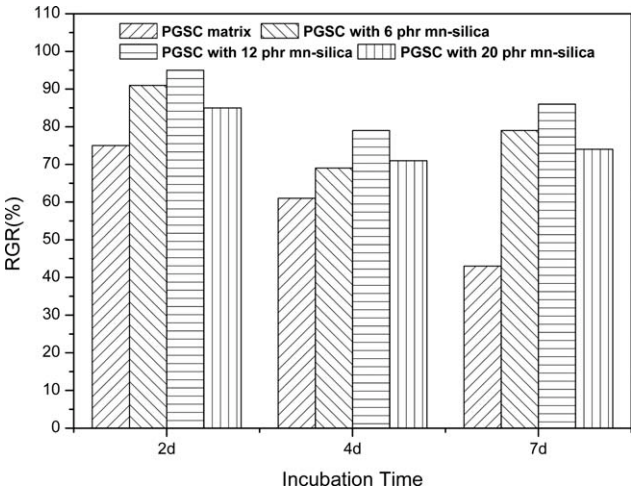

Figure 8 RGR values of representative composites at different incubation time.

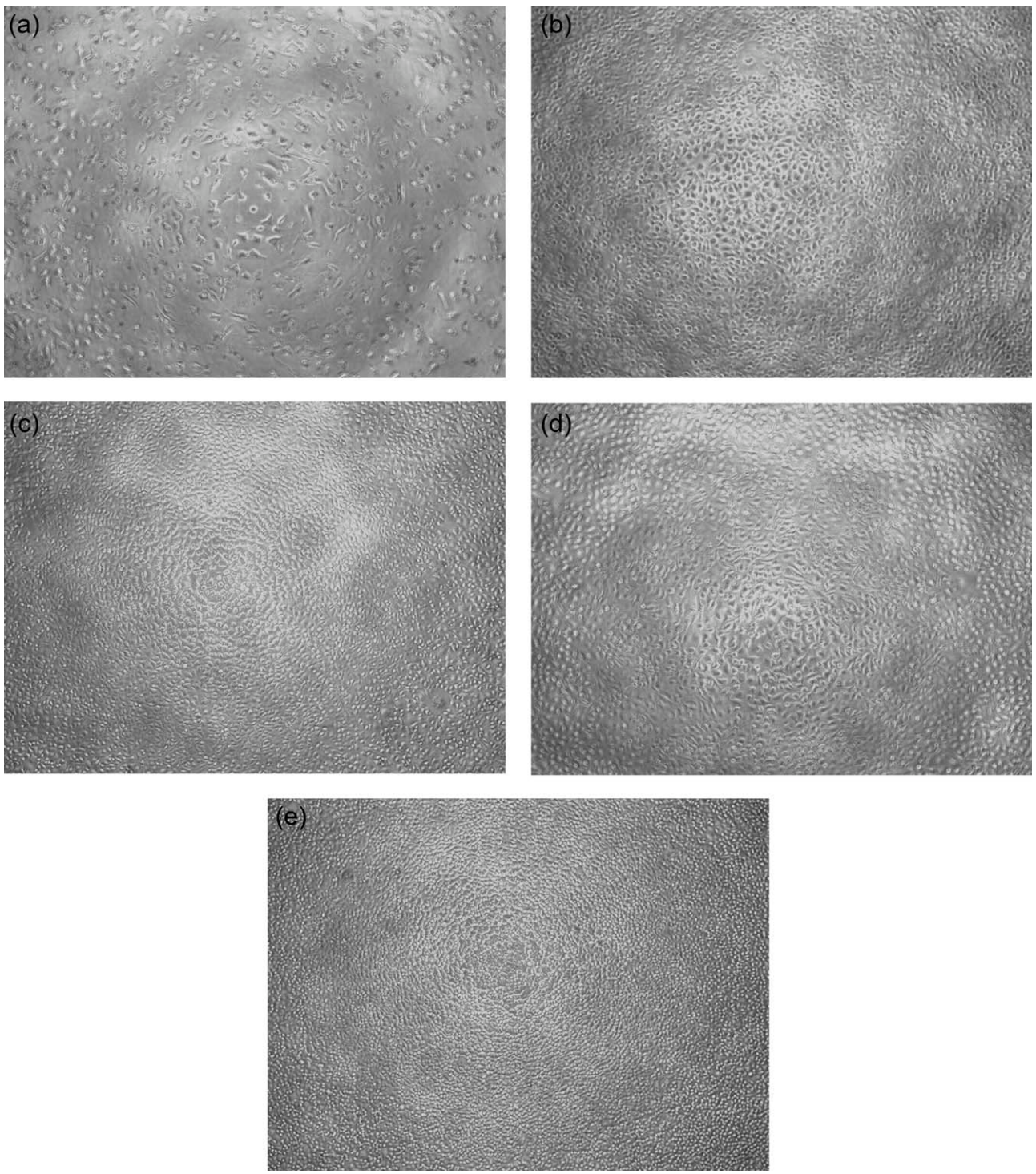

Figure 9 Morphologies of L-929 cells after 7 days' incubation in the negative control and extract solutions of representative composites. (a) neat elastomers; (b) 6 phr; (c) 12 phr; (d) 20 phr; (e) the negative control.

with lower molecular weights quickly dissolved out from the elastomers, leading to the quick weight loss in the first stage; the sol content decreased while the gels was comparatively stable, which accounted for the appearance of the equilibrium stage; with the hydrolysis of ester bonds, the gels degraded into sols and dissolved gradually, resulting in further degradation.

It can be observed that the composites presented comparable degradation rates with neat elastomers at the beginning period, but accelerating degradation at the later periods. After all, crosslinking and

ordered structure played the major role of preventing water from permeating. The mn-silica decreased the chemical crosslinking density and hindered the formation of ordered structure, as mentioned above, thus allowed more water molecules to penetrate into the structure, leading to accelerating degradation.

Liu et al.[24] observed different degradation rules when introducing multi-walled carbon nanotube (MWCNT) to PGSC elastomers. The degradation rates of MWCNT/PGSC composites decreased with the increase of MWCNT loadings, which varied from 0 to 3 wt %. The difference resulted from the particularity and loadings of fillers, and preparation process as well. Abundant hydroxyl groups endow mn-silica strong interactions with polymers or degradation medium while MWCNT is relatively inert; larger loadings (0–17 wt %) of mn-silica had greater effect on the crosslinking density and ordered structure of polymers than MWCNT (0–3 wt %); mn-silica was introduced to the system at the very beginning of synthesis, which interrupted polymer condensation longer than MWCNT. Therefore, degradation rates of elastomers increased by mn-silica, but decreased by MWCNT. In conclusion, degradation rates of this kind of nanocomposites can be adjusted by introducing different kinds of fillers with various loadings, which further widens biomedical applications of the elastomers, such as guided tissue regeneration, prevention membrane of postoperative adhesion, and controlled drug release carriers.

Cytotoxicity assay

To evaluate the possible cytotoxicity of the resulted SiO_2/PPSC composites, the cell viability of L929 cells cultured with their extracts was assessed using MTT assay according to the GB/T16175-1996 standard. The OD value reflects the number of live cells directly. Thus RGR based on the OD value indicates the comparative viability of cells compared to the negative control. The cytotoxicity of materials can be classified into six grades (Table III) according to RGR values: the grade 0 and 1 are accepted as the qualified and show that materials present no or weak cytotoxicity; the grade 2 needs further consideration by combining with the morphology of cells; other grades are treated as the unqualified and suggest that materials present strong cytotoxicity.

RGR values of the representative composites at different incubation time were depicted in Figure 8. The RGR of neat elastomers decreased with time and corresponded to grade 3 after 7 days, which indicated that elastomers presented strong cytotoxicity. The composites with 6 or 12 phr mn-silica belonged to grade 1, which meant that they imparted weak cytotoxicity effect to the cells. The RGR of the composites with 20 phr mn-silica was 74% at the incubation time of 7 days, which was quite close to grade 1. Therefore, the cytotoxicity of PGSC elastomers was greatly weakened due to the introduction of mn-silica. We hypothesized that mn-silica may serve as a buffer to the acidic functional groups and products generated from PGSC degradation, alleviating the toxicity to cells. Ameer and coworkers proposed a similar mechanism to explain slowed degradation of POC/HA composites.[31] Yet these hypotheses need further verification.

The morphologies of L-929 cells incubated for 7 days in the negative control and extract solutions of the representative composites were observed, as shown in Figure 9(a–e). The cells in Figure 9(a) are flat type, which means bad growth state. Seen from Figure 9(b–d), the cells become stereo and present various shapes, such as round, triangle etc., which indicates that the cells are in good condition, yet the cell densities are not as large as the negative control. In conclusion, the cytotoxicity assay indicated that the introduction of mn-silica was beneficial to improving the biocompatibility of elastomers and the composites could be accepted as qualified biomedical materials.

CONCLUSIONS

Series of mn-SiO_2/PGSC were prepared by the *in situ* polymerization and surface modification. Mechanical properties of PGSC elastomers were prominently improved due to the strong filler–polymer interaction and nano-scale network of mn-silica. In particular, the tensile strength improved from 0.9 MPa to 5.3 MPa when 20 phr mn-silica was introduced, which was 489% higher than that of unfilled elastomer. The degradation rates of the composites could be adjusted by varying the loadings of mn-silica. The introduction of mn-silica weakened the cytotoxicity of elastomers to an accepted level as qualified biomedical materials. All the improvements above offer mn-SiO_2/PGSC a wider range of potential biomedical applications, such as tissue engineering scaffolds, degradable bio-coatings, guided tissue regeneration membrane, and so on.

References

1. Wang, Y.; Ameer, G. A.; Sheppard, B. J.; Langer, R. Nat Biotechnol 2002, 20, 602.
2. Wang, Y.; Kim, Y. M.; Langer, R. J Biomed Mater Res A 2003, 66, 192.
3. Sundback, C. A.; Shyu, J. Y.; Wang, Y. D. Biomaterials 2005, 26, 5454.
4. Bettinger, C. J.; Weinberg, E. J.; Kulig, K. M.; Langer, R. Adv Mater 2006, 18, 165.
5. Nijst, C. L. E.; Bruggeman, J. P.; Karp, J. M.; Langer, R. Biomacromolecules 2007, 8, 3067.
6. Liu, Q. Y.; Tian, M.; Shi, R.; Zhang, L. Q. J Appl Polym Sci 2005, 98, 2033.

7. Ding, T.; Liu, Q. Y.; Shi, R.; Zhang, L. Q. Polym Degrad Stab 2006, 91, 733.
8. Liu, Q. Y.; Tian, M.; Ding, T.; Zhang, L. Q. J Appl Polym Sci 2007, 103, 1412.
9. Liu, Q. Y.; Tian, M.; Shi, R.; Zhang, L. Q. J Appl Polym Sci 2007, 104, 1131.
10. Bruggeman, J. P.; Bettinger, C. J.; Nijst, C. L. E.; Langer, R. Adv Mater 2008, 20, 1922.
11. Bruggeman, J. P.; Bettinger, C. J.; Langer, R. Biomaterials 2008, 29, 4726.
12. Yang, J.; Webb, A. R.; Ameer, G. A. Adv Mater 2004, 16, 511.
13. Yang, J.; Webb, A. R.; Hageman, G.; Ameer, G. A. Biomaterials 2006, 27, 1889.
14. Djordjevic, I.; Choudhury, N. R.; Dutta, N. K.; Kumar, S. Polymer 2009, 50, 1682.
15. Kweon, H. Y.; Yoo, M. K.; Kim, T. H.; Cho, S. Biomaterials 2003, 24, 801.
16. Nagata, M.; Tanabe, T.; Sakai, W.; Tsutsumi, N. Polymer 2008; 49, 1506.
17. Lei, L. J.; Ding, T.; Shi, R.; Zhang, L. Q. Polym Degrad Stab 2007, 92, 389.
18. Liu, Q. Y.; Wu, S. Z.; Tan, T. W.; Zhang, L. Q. J Biomater Sci Polym Ed 2009, 20, 1567.
19. Liu, Q. Y.; Tan, T. W.; Zhang, L. Q. Biomed Mater 2009, 4, 025015.
20. Edwards, D. C. J Mater Sci 1990, 25, 4175.
21. Zhang, L. Q.; Wu, Y. P.; Wang, Y. Q.; Wang, Y. Z. China Synth Rubber Ind 2000, 2, 8.
22. Hamed, G. R. Rubber Chem Technol 2007, 80, 533.
23. Wang, Z. H.; Liu, J.; Wu, S. Z.; Zhang, L. Q. Phys Chem Chem Phys 2010, 12, 3014.
24. Liu, Q. Y.; Wu, J. Y.; Tian, W.; Zhang, L. Q. Polym Degrad Stab 2009, 94, 1427.
25. Lei, L. J.; Li, L.; Zhang, L. Q.; Chen, D. F. Polym Degrad Stab 2009, 94, 1494.
26. Chen, C. G.; Justice, R. S.; Schaefer, D. W.; Baur, J. W. Polymer 2008, 49, 3805.
27. Aso, O.; Eguiazabal, J. I.; Nazabal, J. Compos Sci Technol 2007, 67, 2854.
28. Barus, S.; Zanetti, M.; Lazzari, M.; Costa, L. Polymer 2009, 50, 2595.
29. Chen, Y. T.; Liu, L.; Wu, L. M. Silic Fluor Inform 2005, 1, 30.
30. Shi, R.; Ding, T.; Liu, Q. Y.; Zhang, L. Q. Polym Degrad Stab 2006, 91, 3289.
31. Qiu, H. J.; Yang, J.; Kodali, P.; Ameer, G. A. Biomaterials 2006, 27, 5845.